



South Atlantic deep eastern boundary current driven by Agulhas rings: An idealized study

Xiaoting Yang^{a,*}, Eli Tziperman^{b,a}

^a Department of Earth and Planetary Sciences, Harvard University, 20 Oxford st, Cambridge, MA, USA

^b School of Engineering and Applied Sciences, Harvard University, 20 Oxford st, Cambridge, MA, USA



ARTICLE INFO

Keywords:

Deep eastern boundary currents
North Atlantic deep water outflow
Vorticity budget
Eddy stretching transport

ABSTRACT

The deep eastern boundary current (DEBC) in the southeast Atlantic Ocean plays an important role in the global meridional overturning circulation, by carrying a comparable fraction of the North Atlantic Deep Water transport toward the Southern Ocean to that of the deep western boundary current. At the same time, the southeast Atlantic Ocean is constantly influenced by energetic Agulhas rings that are shedded by the Agulhas current. It has been pointed out that the eddy thickness transport by these Agulhas rings is important in enabling the deep water mass that flows southeastward within the interior of the South Atlantic Ocean to cross isolines of large scale potential vorticity toward the eastern boundary where it feeds the DEBC. In this work, we focus on the dynamics of DEBC itself which carries this water mass into the Southern Ocean. We use idealized general circulation model configurations to study the relationship between the Agulhas rings, bathymetry and the southward DEBC in southeast Atlantic Ocean. We find that a DEBC comparable to that in observations and state estimate products is obtained only with combined forcing by Agulhas rings and a sloping bathymetry. The DEBC is then characterized by a mid-depth core at a 2.2 km, again similar to observations. We analyze the momentum and vorticity budgets of the DEBC and show that it is driven by vortex stretching that is sensitive to both eddy temperature transport and the bottom slope.

1. Introduction

The southward spreading of the North Atlantic Deep Water (NADW) is an important branch of the global meridional overturning circulation that connects the North Atlantic Ocean and the Southern Ocean (Lumpkin and Speer, 2007). The NADW flows southward mainly as the deep western boundary current (DWBC) in the Atlantic Ocean (Stommel and Arons, 1959). However, the DWBC has been found to bifurcate twice, near the equator and near 22°S in the South Atlantic Ocean, and form eastward zonal flows (Weiss et al., 1985; Böning and Schott, 1993; Speer et al., 1995; Stramma and England, 1999; Hogg and Thurnherr, 2005). Tracer distributions, such as salinity, oxygen and nutrients at about 2 km depth, are found to form tongue-like structures near the eastern boundary of the southeast Atlantic Ocean, implying a southward flow of a water mass with characteristics of NADW (Warren and Speer, 1991; Saunders and King, 1995; Speer et al., 1996; Arhan et al., 2003). Non-negligible southward transports near the eastern boundary in the NADW layer of about 6 Sv at 11°S (Speer et al., 1996), and about 10 Sv near the southern tip of the African continent (Saunders and King, 1995; Arhan et al., 2003) have been found. These transports are carried mainly by a concentrated deep eastern boundary current

(DEBC) between 1 and 4 km depth, with a core magnitude of about 3 cm/s (Yang et al., 2020a).

The zonal pathway of the NADW across the South Atlantic Ocean was found by Sebille et al. (2012) to be driven by eddy thickness flux due to energetic Agulhas rings that propagate into the South Atlantic Ocean from its southern boundary. These eddies allow the water mass to cross isolines of large-scale potential vorticity and flow southeastward, creating a broad flow toward the southeast boundary of the South Atlantic. However, Sebille et al. (2012) did not consider the dynamics of the concentrated DEBC near the eastern boundary itself that is fed by this broad flow. In a recent regional simulation of the southeast Atlantic flow field, the DEBC was found to be balanced by linear vortex stretching ($\beta v \approx f \partial_z w$), mainly driven by eddy temperature mixing and by the bathymetry (Yang et al., 2020a). However, in a study using an idealized GCM configuration (Yang et al., 2021), the DEBC forced by a time-mean inflow/outflow boundary conditions with a slope bathymetry but no eddies, has a *bottom-intensified* vertical structure, which is different from the *mid-depth current core* simulated in the Southern Ocean State Estimate (SOSE, Mazloff et al., 2010) and by the realistic regional simulation of Yang et al. (2020a). This suggests the importance of eddies in the dynamics of the DEBC in the southeast

* Corresponding author.

E-mail address: xiaoting_yang@g.harvard.edu (X. Yang).

Atlantic Ocean, similar to their important role in driving the interior flows toward the eastern boundary, motivating the present work which complements and extends the findings of Yang et al. (2021).

In this work, we use a simplified configuration of the southeast Atlantic Ocean which includes a representation of Agulhas rings on the southern boundary, and focus on the effect of these Agulhas rings and bathymetry on the formation of a deep southward current near the eastern boundary. We find that the configuration including both the idealized Agulhas rings and a sloping bottom simulates a realistic-looking DEBC with a mid-depth core, as opposed to a bottom-intensified structure found without explicit forcing by Agulhas rings. The structure of the DEBC is sensitive to both the Agulhas rings and bathymetry. This paper is organized as follows. We discuss the model configuration and experiment designs in Section 2. Results are presented in Section 3, which includes a comparison between different experiments (3.1), a discussion of time variability of the DEBC (3.2), and its vorticity dynamics (3.3). We conclude in Section 4.

2. Methods

We use idealized configurations, representing the southeast Atlantic Ocean, of the Massachusetts Institute of Technology General Circulation model (MITgcm, Marshall et al., 1997). The horizontal resolution is 0.1° in the zonal direction and $0.1^\circ \times \cos \theta$ in the meridional direction (θ is latitude), making the grid cells nearly square. There are 57 vertical levels whose thickness ranges from 5 m near the surface to 125 m near the bottom. The model domain is 26.3° wide in the zonal direction, and the latitudinal range is from 38°S to 25°S . Two bathymetry profiles of the eastern boundary are used in the experiments. The first is a polynomial fit to the realistic eastern boundary topography of the southeast Atlantic Ocean at 30°S (Supplementary Fig. 1a, gray shading). To isolate the effects of the bathymetric slope, a flat bottom case is also used (Supplementary Fig. 1b, gray shading). The eastern continental boundary in all scenarios is tilted northwestward in the meridional direction, similar to the realistic western coastline of the South African continent.

Open boundaries are used at the north, south and west where boundary conditions are specified. Time-mean southward outflow against the eastern boundary between one and four kilometers depth has been indicated by tracer observations (Warren and Speer, 1991; Arhan et al., 2003) and found on the southern boundary of this specific domain in SOSE (Yang et al., 2020a). As an idealization, a core of southward flow is specified on the southern boundary that has Gaussian structures in both the zonal and the vertical directions, with the core depth at 2.5 km and a core speed of 5 cm/s (Supplementary Fig. 1a,b), and its core longitude is 3 degrees westward of the solid boundary at the core depth, comparable to the averaged outflow core speed in the southeast Atlantic Ocean in both SOSE and the regional Atlantic simulations of Yang et al. (2020a). Similar outflow boundary conditions have been used by Yang et al. (2021) to simulate non-eddy DEBCs. The time-mean meridional velocity on the southern boundary away from the eastern boundary is set to zero for simplicity. We compensate for the total transport out of the southern boundary (both the mean flow and time-dependent Agulhas rings described below) with a weak inflow from the western boundary, uniform in depth and latitude, motivated by the SOSE results that show such an eastward inflow toward the DEBC area.

The monthly v -velocity field at 2.2 km depth, 38°S from SOSE over a period of six years shows eddy signal with a timescale of about four months (Supplementary Fig. 2, colored lines). Therefore, idealized Agulhas rings (“IAR” in abbreviation) are specified on the southern boundary at monthly intervals. The temporal and zonal structure of the idealized Agulhas rings is simplified as a westward decaying and propagating signal,

$$v(x, z, n) = v_0 \exp(z/D) \cos [-(x - x_E)/L_1 + (n - 1)\pi/2] \exp [(x - x_E)/L_2],$$

in which x_E is the position of the eastern boundary, $L_1 = 35$ km is the wavelength of the propagating rings, $L_2 = 22$ km is the decay scale, and n is the month number ($n \in [1, 2, \dots, 12]$, Supplementary Fig.1c). These simplified structures capture the magnitude and the most important large-scale features of the SOSE flow field reasonably well (Supplementary Fig. 2). The vertical structure of these Agulhas-like rings is an exponential decay with a vertical scale of $D = 2$ km (Supplementary Fig. 1d). The magnitude of the eddy flow at the surface is 1 m/s, the same order of magnitude of Agulhas ring velocities in SOSE. Later we will show that these boundary conditions produce Agulhas-like rings of surface magnitude and propagation paths in the interior of the model domain comparable to those in SOSE. In these experiments, we use a linear equation of state, where the density is a function of temperature only ($\rho = \rho_0 [1 - \alpha (T - T_0)]$, $\rho_0 = 1025$ kg/m³, $T_0 = 10^\circ\text{C}$, $\alpha = 1.668 \times 10^{-4} \text{ }^\circ\text{C}^{-1}$). For the boundary conditions, the temperature field is perturbed from a reference temperature profile that is the zonal average at the northern boundary of the corresponding domain in SOSE, such that the density is always in thermal wind balance with the specified flow field. Since our focus is the effect of the rings forced at the southern boundary, we simplify the surface forcing such that there is no wind forcing, and the SST is restored to a uniform constant of 18°C on a timescale of 10 days.

We use horizontal harmonic viscosity $A_h = 10$ m²/s, horizontal bi-harmonic viscosity $A_4 = 10^{10}$ m⁴/s and vertical viscosity $A_v = 10^{-4}$ m²/s. The Gent–McWilliams scheme (Gent and McWilliams, 1990) is used with $\kappa_{GM} = 20$ m²/s, a bi-harmonic diffusivity is specified $\kappa_4 = 10^{10}$ m⁴/s, and the vertical diffusivity is $\kappa_v = 10^{-5}$ m²/s. We also use a linear bottom drag ($r = 10^{-3} \text{ s}^{-1}$) and “no-slip” condition on the horizontal boundary. We choose these parameters to be similar to those used in SOSE integrations which are also eddy-resolving, although at a twice coarser horizontal resolution than used here. Using “free-slip” boundary condition was found not to make a significant difference to the result (Supplementary Fig. 4). Finally, we use the 33 advection scheme of MITgcm (3rd order DST Flux Limiter).

To compare the roles of eddies and bathymetry in the dynamics of the deep southward outflow near the eastern boundary, four experiments are used: the “Slope+rings” case uses the slope bathymetry and prescribes a mean flow plus idealized Agulhas rings as southern boundary conditions (this is the most realistic configuration); the “Slope” case uses the slope bathymetry but has only a mean flow forced on the southern boundary; the “Flat bottom+rings” and the “Flat bottom” experiments complete the set. When we do not impose IARs on the southern boundary, the simulated interior flow is weak and does not generate strong eddies; One might argue for making the viscosity and diffusivity parameters larger in these experiments to account for the missing role played by the resolved eddies. But we choose to use the same parameters, for the direct comparison between cases to be more meaningful.

To further verify that it is the Agulhas rings, rather than other eddy motions, that are important for driving and determining the vertical structures of the DEBC, we carried out additional experiments in which we allow eddies to develop, by adding to our control “Slope+rings” case, (1) a meridionally dependent SST forcing; (2) horizontally dependent zonal and meridional wind stresses; (3) both horizontally dependent SST and wind forcings (Supplementary Fig. 5). The forcing terms used in these idealized experiments are based on time-mean of the Comprehensive Ocean–Atmosphere Data Set (Woodruff et al., 1987, COADS,) which was also used to study the DEBCs in realistic model configurations (Yang et al., 2020a). The SST forcing is taken to be the zonal average of the time-mean SST in the corresponding domain from COADS (Supplementary Fig. 5d). The zonal and meridional wind stresses are taken from COADS for the Southeast Atlantic (Supplementary Figs. 5e,f). Furthermore, we also carried out an experiment in which we added the surface forcing of both SST and wind stresses to the “slope” case which does not include the IARs (“slope+surf frc” case). To also separate the role played by the imposed weak mean flow in

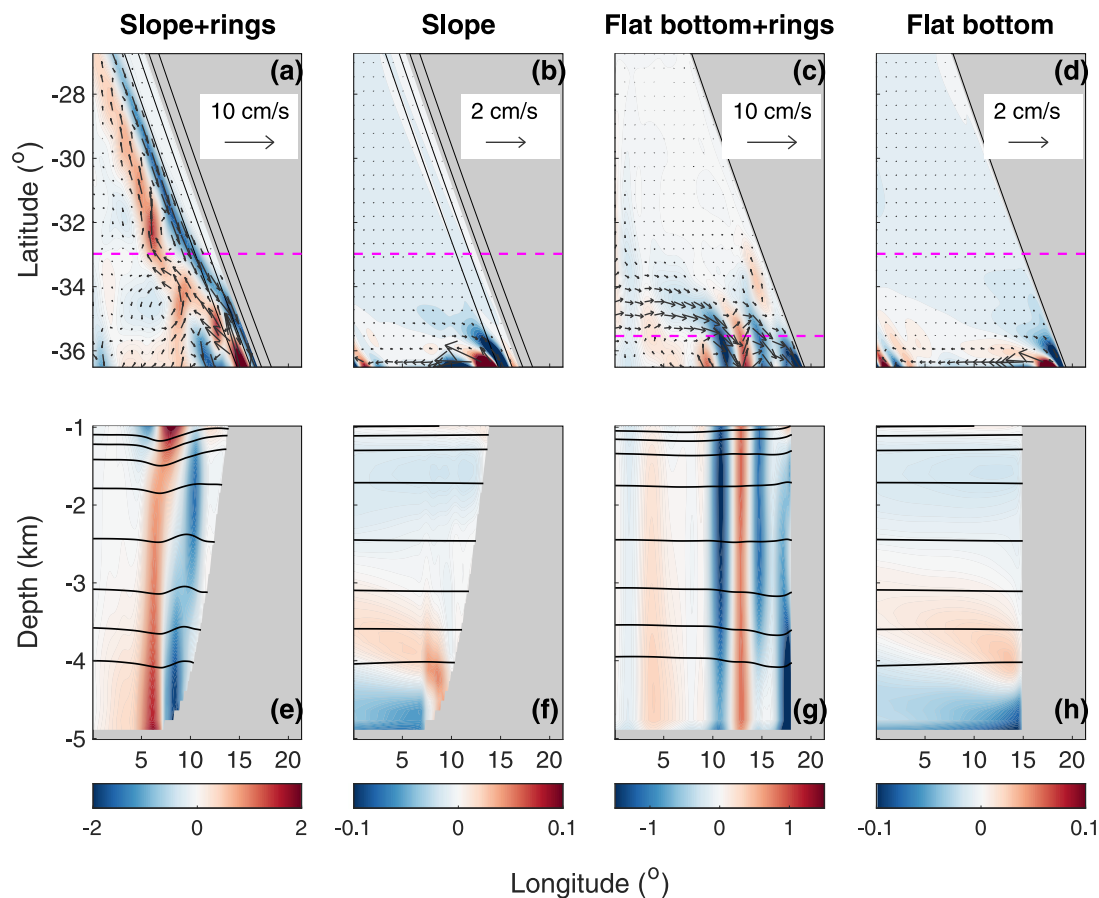


Fig. 1. Steady-state flow field of the four experiments showing that a realistic-like DEBC is obtained only when both a bottom slope and idealized Agulhas ring forcing are included. Upper panels: horizontal maps of meridional velocity (colors, cm/s), velocity vectors (black arrows) at a depth of 2.2 km, with bathymetry shown by the black contours. Lower panels: zonal sections of meridional velocity (colors, cm/s), and isopycnal surfaces (black contours, σ density values between 27.98 kg/m³ and 28.45 kg/m³, with an interval of 0.07 kg/m³). The zonal sections are take at latitude of 33°S in panels e,f,h and 35.5°S for panel g. The gray patches indicate the location of land and the purple lines in the upper panels show the latitudes of the zonal sections. (a,e) “Slope+rings” case; (b,f) “Slope” case; (c,g) “Flat bottom+rings” case; (d,h) “Flat bottom” case.

the southern boundary conditions, another version of “slope+rings” without such a mean flow was also carried out (“no mean flow”). [Table 1](#) summarizes the configurations of these experiments.

Each experiment is integrated to a statistical steady state (averaged temperatures over different depth ranges converge). For the analysis presented in the following, all the time-mean fields are averaged over 20 years of integration past the point of statistical steady state, and all the nonlinear terms are calculated using bi-daily data over the same 20 years. The figures analyzing the results do not include the 20 grid points closest to the southern/northern/western boundaries, where artifacts of the boundary conditions exist, such as concentrated meridional flow near the western boundary where a zonal inflow is prescribed.

3. Results

In this section, we compare the four cases 1–4 in [Table 1](#), to demonstrate the importance of both the idealized Agulhas rings and a sloping bathymetry in the dynamics of the South Atlantic DEBC (Section 3.1). In the following two subsections, we focus on the “Slope+rings” case which is the simplest configuration that can still lead to a realistic DEBC. First, in order to verify that our results are relevant to the actual South Atlantic DEBC, we analyze the time-variability of the DEBC in Section 3.2 and demonstrate that the idealized DEBC shows similarity to the DEBC in more realistic configurations in terms of its statistic characteristics and momentum budget. Then, in Section 3.3, we discuss the vorticity dynamics of this DEBC and show that the DEBC simulated in the “Slope+rings” is forced by vortex stretching

Table 1

Case name and corresponding model configurations (bathymetry and boundary forcing).

Case name	Model configuration
1 “Slope+rings”	Slope + mean flow + idealized Agulhas rings
2 “Slope”	Slope + mean flow
3 “Flat bottom+rings”	Flat bottom + mean flow + idealized Agulhas rings
4 “Flat bottom”	Flat bottom + mean flow
5 “Slope+rings+surf frc”	Slope + idealized Agulhas rings + mean flow + SST and wind forcing
6 “Slope+surf frc”	Slope + mean flow + SST and wind forcing
7 “No mean flow”	Slope + idealized Agulhas rings

driven by eddy temperature transport (Section 3.3). We find that there are two branches of the DEBC, similar to those simulated in realistic configurations and SOSE, one near the eastern boundary at mid-depth (1–3 km) and another that is bottom intensified (below 3 km) and further to the west, near the western edge of the slope. We further discuss the different vertical structures of the two branches and the mechanisms responsible for these structures in Supplementary material.

3.1. Time-averaged flow field

[Fig. 1](#) shows the time-mean flow field at the steady state of cases 1–4. In the “Slope+rings” case which is the most realistic-like of these first four runs, there is a southward DEBC between one and four kilometers depth eastward of 10°E ([Fig. 1a,e](#)). The core depth is at 2.2 km depth and a core speed of 2 cm/s, comparable to the speed

of the DEBCs in SOSE and in a realistic regional simulation using the MITgcm (Yang et al., 2020a, hereafter YTS). The core width is comparable to the width of the slope. The isopycnals tilt upward above the current core and downward below the current core, which implies that this flow is a local minimum of large-scale potential vorticity ($f\partial_z\sigma$), again consistent with the results of SOSE and YTS. At its core depth, there is northward flow west of the southward DEBC, which is a combination of a surface-intensified signal and a bottom-intensified signal (red in Fig. 1e), and this northward flow does not show a core at mid-depth as does the southward DEBC. There is another branch of southward flow below 3 km depth which is bottom-intensified (Fig. 1e, at longitude 10, below 3 km depth). Such bottom intensified DEBCs have also been observed in SOSE and YTS, where the slope connects with the relatively flat ocean floor.

There are no concentrated flows near the eastern boundary when idealized Agulhas rings are removed from the southern boundary condition, as seen for example in the “Slope” case. Furthermore, the interior flows are generally weak in this case (Fig. 1b,f), even though the mean flow boundary condition is still imposed and the slope bathymetry still used. A weak concentrated southward flow is found only very close to the specified outflow condition (Fig. 1b,f).

The DEBC in the “Flat bottom+rings” case is of magnitude 1.5 cm/s, almost as strong as that in the more realistic “Slope+rings” case, but is confined to a very small latitudinal range of the domain, southward of 34°S (Fig. 1c,g), and it is clearly fed by an eastward interior zonal flow between 34°S and 36°S. The southward flows near the eastern boundary are composed of two parts (Fig. 1g): Near 15°E, there is a core of southward flow that is detached from the bottom, while very close to the eastern boundary (eastward of 15°E), there is a very weak mid-depth core at 2 km depth and a strong bottom-intensified southward flow. None of these branches is similar to the more realistic DEBC seen in the “Slope+rings” case in Fig. 1e. When both idealized Agulhas rings and slope bathymetry are removed from the configuration (“Flat bottom” case), there is again no concentrated flow near the eastern boundary, except very close to the southern boundary, due to the direct influence of the mean flow boundary condition (Fig. 1d,h).

In summary, a combination of a sloping bathymetry and idealized Agulhas rings is required to produce a coherent southward DEBC between one and four kilometers depth, with a vertical structure detached from the bottom and a width comparable to the sloping bathymetry, as seen in realistic simulations and SOSE.

These results can explain the deficiencies in the idealized DEBC simulations in Yang et al. (2021) in which DEBCs were forced using strong steady southward inflow/outflow near the eastern boundary. In Yang et al. (2021), the DEBC above the same slope used here only shows the bottom-intensified branch with no mid-depth current core. We can now interpret this as being due to the lack of Agulhas ring forcing from the southern boundary in that study. Interestingly, the idealized simulations in Yang et al. (2021) of the South Pacific and Indian Ocean DEBCs were more successful, suggesting that eddy driving is important mostly for the South Atlantic DEBC. Below we show that the eddy fluxes of vorticity and temperature by such rings are important for maintaining the mid-depth branch of southward flows observed in the “Slope+rings” case. This seems to complement the results of Sebille et al. (2012) who found these rings to be important for driving southeastward interior flows toward the eastern boundary.

We have so far demonstrated the importance of the Agulhas rings in driving the DEBCs, yet we need to verify that it is indeed these rings rather than other eddy motions that drive and determine the vertical structure of the DEBC. The presence and importance of eddies for the upper ocean eastern boundary currents which are driven by the surface meridional temperature gradient and surface wind stresses has long been studied (Peliz et al., 2003; Cessi and Wolfe, 2009; Colas et al., 2011; Kurian et al., 2011; Bire and Wolfe, 2018). To allow local eddy activity to develop, we add meridional SST gradients and

surface wind (Section 2) to several model configurations. First, when these are added to a configuration without the idealized Agulhas rings (“Slope+surf frc”), the eddy kinetic energy is much smaller than that due to the Agulhas rings (compare Fig. 3a,f,k and e,j,o). The eddy kinetic energy of the idealized Agulhas rings within the model domain away from the southern boundary is comparable to that observed in SOSE in the southeast Atlantic ocean, both near the surface and at depth (Compare Fig. 3a,f and Supplementary Fig. 9). The weaker eddy kinetic energy forced by surface forcings alone is also comparable to that observed in SOSE in the southeastern Indian and Pacific Oceans which are not influenced by the energetic Agulhas rings (compare Fig. 3e and Supplementary Figs. 10 and 11). This suggests that the local eddy generation in our model with such surface forcings is realistic. No DEBC is observed in the case with surface forcings and without Agulhas rings (Fig. 2d,h), due to the weakness of the locally forced eddies near the eastern boundary, which do not penetrate into the deep ocean (Fig. 3e,j,o).

When we add, in experiment 5 in Table 1, the wind and SST gradients to the control run (“slope+rings”) that also contains the Agulhas rings, the change to the eddy activity is not large, yet shows a secondary peak in the zonal sections very close to the eastern boundary, in addition to the main peak along the pathway of the idealized Agulhas rings (Fig. 3c,h,m). The addition of such surface forcings does not lead to any significant changes to the DEBCs that we are primarily interested in here (Fig. 2b,f).

Another experiment (case 7 in Table 1) was also carried out to test the role played by the weak mean flow imposed on the southern boundary in addition to the time-varying idealized rings. When such a mean flow is removed but the bathymetric slope and idealized ring forcing are still used, we observe that the DEBC weakens fairly dramatically along its entire length. It still has the right mid-depth vertical structure (Fig. 2c,g). This verifies the importance of both the weak mean flow boundary forcing and eddy forcing, in setting the amplitude and vertical structure of the DEBC.

3.2. Time-variability of the “Slope+rings” case

We found that Agulhas-like rings forced by the southern boundary condition are a critical part of the southeast Atlantic DEBC dynamics. We now would like to show that the variability of the DEBC, which is induced by the ring forcing, is similar to that found in realistic simulation. We conclude that the rings are critical not only to the time-mean DEBC characteristics, but also to its variability. We focus for this purpose on the “Slope+rings” case.

Fig. 4c,f compares the magnitude of the eddy velocity ($V_{eddy} = \sqrt{u'^2 + v'^2}$, shading) and the mean meridional flow (contours). The patch of high-value of V_{eddy} shows the propagation path of the Agulhas-like rings, which coincides with the position of the northward mean flow (see also Supplementary Fig. 6a). The northwestward propagation speed of the Agulhas-like rings is well-explained by the advection by this northward current (not shown). The core of the southward DEBC exists eastward of the patch of high V_{eddy} . The magnitude of the eddy velocity is larger compared to both the northward and southward mean flows, so that the signal of these currents may not be detectable in instantaneous observations. Supplementary Fig. 6b shows the pdf of the v -velocity at longitude 10°E, latitude 33°S and at a 2.2 km depth, within the core of the time-mean southward DEBC. Both northward and southward velocities are likely to be observable at this position instantaneously, even though the time-mean southward flow is as strong as 2 cm/s. That the idealized current core is eastward of the local maximum of eddy activity, and that the signal of the mean flows is masked by passing eddies are consistent with the southeast Atlantic DEBC in SOSE and YTS. We conclude that this transient nature of this DEBC is forced by the Agulhas rings.

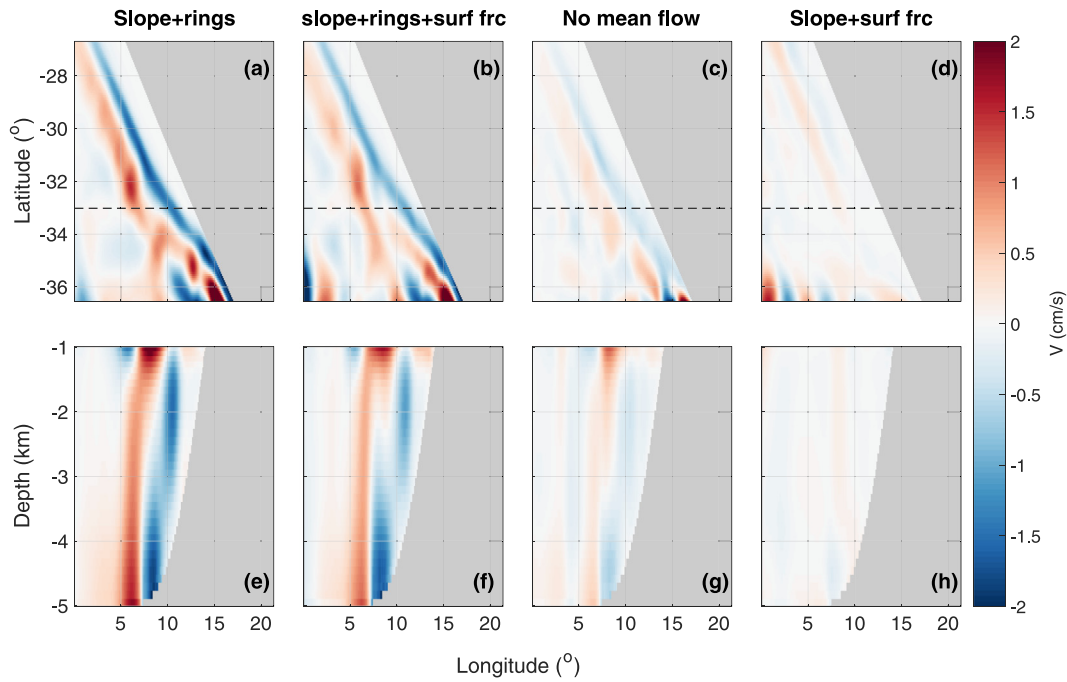


Fig. 2. The deep flow field of the cases based on the control “Slope+rings” case. Upper panels: horizontal maps of northward velocity at 2.2 km depth (cm/s, colors); the land mask (gray patch); the latitude of the zonal sections shown in the lower panels (black dashed line). Lower panels: zonal sections of northward velocity (colors) at the latitude shown by the black dashed line in the upper panel; land mask (gray patch). (a,e) The control “Slope+rings” case; (b,f) the control case forced by horizontally dependent SST and wind forcing; (c,g) The “Slope+rings” case without the mean flow on the southern boundary condition; (d,h) The “slope” case forced by horizontally dependent SST and wind forcing.

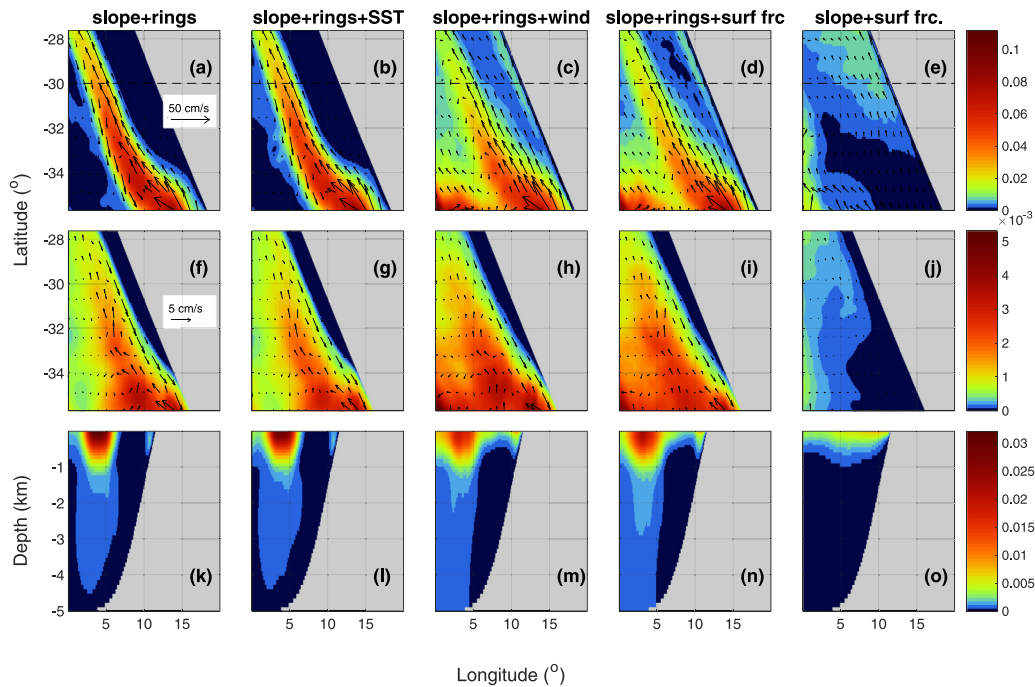


Fig. 3. Top panels: the eddy kinetic energy averaged over the topmost 50 m (colors); the horizontal flow field averaged over the topmost 50 m (black arrows); land mask (gray shading); the latitude of the zonal sections shown at the bottom panels (black dashed line). Middle panels: eddy kinetic energy at 2.2 km depth (colors); horizontal flow field at 2.2 km depth (black arrows); land mask (gray shading). Bottom panels: zonal sections of eddy kinetic energy (colors); land mask (gray shading). (a,f,k) The control “Slope+rings” case; (b,g,l) The “slope+rings” case forced by meridional SST profile; (c,h,m) the “slope+rings” case forced by 2D wind stresses; (d,i,n) the “slope+rings” case forced by surface SST and wins stress forcing; (e,j,o) The “slope” case forced by surface SST and wind stress forcing.

We notice that the maxima of eddy activities in the “Slope+rings” case, both near the surface and at depth (Fig. 3a,f,k), are detached from the solid eastern boundary due to the propagation of the energetic Agulhas rings, even though the maximum of the specified eddy

forcing on the southern boundary is right at the eastern boundary. This detachment of the core of high eddy activity from the eastern boundary is due to the northwestward propagation of the Agulhas rings at some angle to the eastern boundary. This feature is also consistent

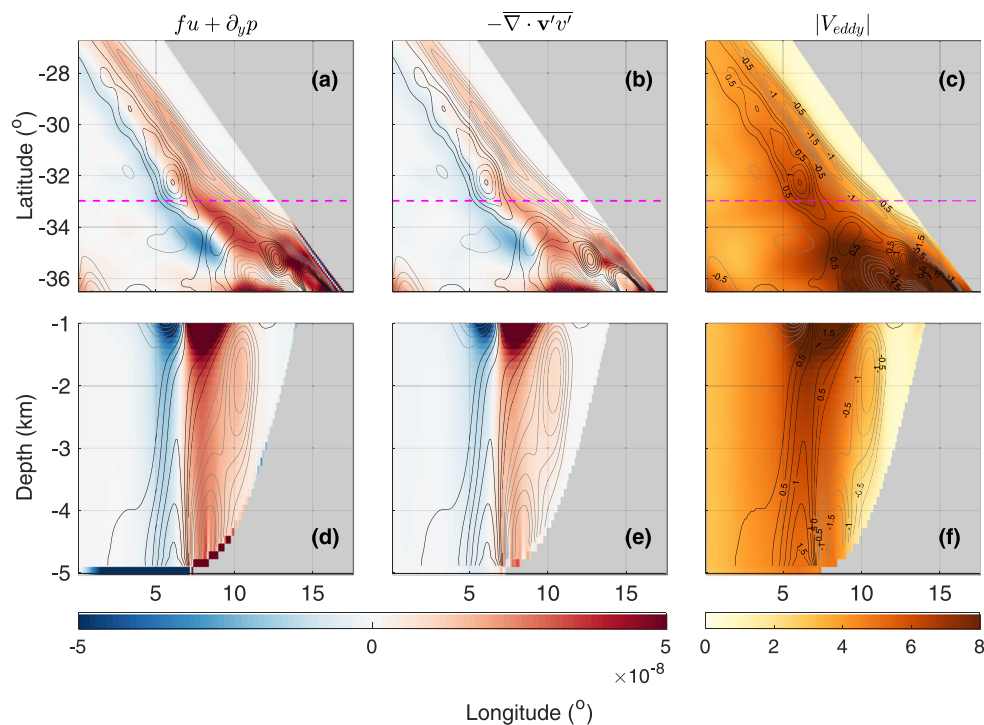


Fig. 4. Momentum budget and magnitude of eddy velocity of the “Slope+rings” case. (a,d) The residual of the geostrophic balance (Coriolis minus pressure accelerations) at a depth of 2.2 km (a), and at latitude of 33°S (d). (b,e) The divergence of eddy v -momentum fluxes at depth of 2.2 km (b), and at latitude of 33°S (e). (c,f) Magnitude of eddy velocity ($\sqrt{u'^2 + v'^2}$, cm/s) at depth of 2.2 km (c), and at latitude of 33°S (f). In each panel, the gray patch indicates the location of land, and the purple lines in the upper panels show the latitudes of the vertical sections. The dark gray contours show northward v -velocity (cm/s); the light gray contours show southward v -velocity (cm/s). Contours are drawn for v -velocity between 0.25 cm/s and 1.5 cm/s, with an interval of 0.25 cm/s.

with SOSE (Supplementary Fig. 9) and the findings of YTS. The peak eddy kinetic energy occurs over a relatively flat bottom in this case, and that means that conceptual models for near-surface eastern boundary currents (e.g., Csanady, 1978, 1985; Furue et al., 2013) would need to take that into account in their solution above the flat bottom, when applied to the southeast Atlantic Ocean.

Analysis of the v momentum equation shows that the two dominant terms in the DEBC region are the Coriolis term and the pressure gradient term (geostrophy), whose residual is balanced by the eddy momentum flux divergence $-\nabla \cdot \overline{v'v'}$ (Fig. 4a,b,d,e). In the DEBC region, the eddy momentum flux divergence tendency is northward, which means that the eddies are slowing the southward mean current down, instead of forcing such a current. This is also consistent with the findings of YTS.

The analysis of the time-variability of the DEBC in the “Slope+rings” case, which is the most realistic configuration of those without surface forcings considered here, shows three features consistent with SOSE and YTS. First, the core of the idealized DEBC is eastward of the local eddy activity maxima. Second, the eddy variability is still sufficiently large to mask the presence of the time-mean current instantaneously. Third, the eddy momentum transport acts as a drag on the southward time-mean DEBC. This consistency suggests that our explanation of the dynamics of this idealized DEBC, and in particular the role of Agulhas rings in driving it, is also relevant for the observed South Atlantic DEBC. That was not the case for the idealized study of Yang et al. (2021) because it did not include Agulhas rings and was therefore not able to simulate a DEBC with a vertical structure consistent with SOSE.

3.3. Vorticity dynamics of the DEBC

We found so far that the both the Agulhas rings and continental slope are critical for driving the DEBC. In order to find the driving

mechanism, we follow YTS and consider the relative vorticity equation, derived by taking the curl of the momentum equations,

$$\beta \overline{w} = f \frac{\partial \overline{w}}{\partial z} - \nabla \cdot \overline{v\zeta} - \nabla \cdot \overline{v'\zeta'} + \hat{k} \cdot \nabla \times \overline{\mathbf{F}}. \quad (1)$$

In this equation, $\zeta = \partial_x v - \partial_y u$ is the vertical component of the relative vorticity, w is vertical velocity, and $\beta = 2\Omega \cos \theta / R$ is the meridional gradient of the Coriolis parameter f . The last term, $\hat{k} \cdot \nabla \times \overline{\mathbf{F}}$, stands for the vertical component of the curl of the parameterized horizontal friction.

For the control “Slope+rings” case, the dominant vorticity balance for the DEBC is between advection of planetary vorticity ($\beta \overline{w}$), vertical stretching ($f \partial_z \overline{w}$) and the eddy vorticity transport ($-\nabla \cdot \overline{v'\zeta'}$), all shown in Fig. 5. This is a similar dominant balance to that found in the realistic southeast Atlantic simulation of Yang et al. (2020a) which also included Agulhas ring signals at its southern boundary. As was explained in Yang et al. (2020a), the eddies act as a drag on the southward DEBC in the momentum budget, and at the same time induce a southward DEBC in the vorticity budget through the beta term.

YTS found that the stretching w_z that drives the DEBC is a result of eddy temperature fluxes, and we would like to verify that these eddy fluxes are indeed dominated by the rings forced at the southern boundary, as opposed to other eddy effects included in the realistic simulation of YTS. We use the temperature equation,

$$\frac{\partial \overline{T}}{\partial t} + \overline{w} \frac{N^2}{\alpha g} = -\nabla \cdot \overline{vT'} - \nabla \cdot \overline{v'T'} + \text{diff}, \quad (2)$$

where T is the temperature, $N^2 = -g \partial_z \overline{\rho} / \rho_0$ is the buoyancy frequency, α is the thermal expansion coefficient and diff is the parameterized mixing. Fig. 6 shows the vertical divergence of the vertical velocity, $\partial_z w$, reconstructed from the different terms in Eq. (2). We find that in the core of the DEBC (shown by the contours), the dominant term driving $\partial_z w$, and therefore driving vortex stretching, is the eddy temperature

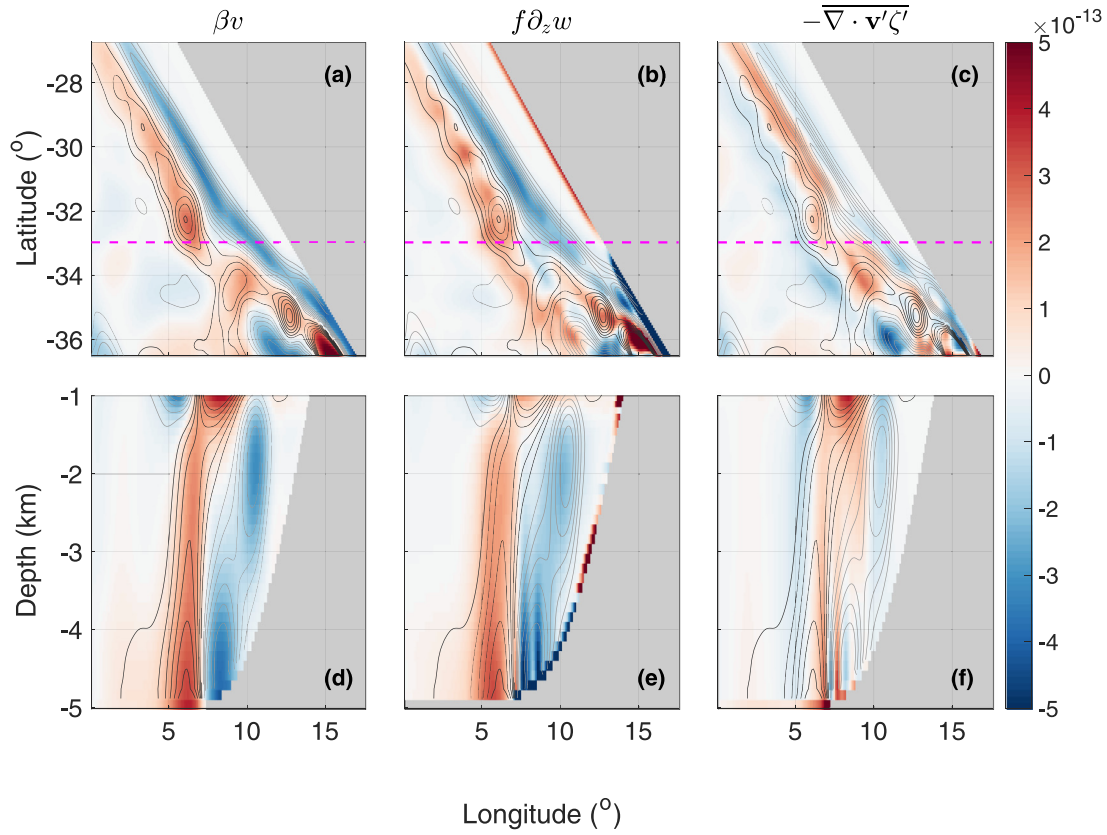


Fig. 5. Dominant terms in the vorticity budget of the “Slope+rings” case. Panels (a,b,c): horizontal maps at a 2.2 km depth; (d,e,f): zonal sections at 33°S. (a,d) advection of planetary vorticity (βv); (b,e) linear vertical stretching ($f \partial_z w$); (c,f) divergence of eddy vorticity fluxes ($-\nabla \cdot \mathbf{v}' \zeta'$). In each panel, the gray patch indicates the location of land, the dark gray contours are northward v -velocity, and the light gray contours are southward v -velocity. The contours are drawn for v -velocity between 0.25 cm/s and 1.5 cm/s, with an interval of 0.25 cm/s. The purple lines in the upper panels show the latitudes of the zonal sections.

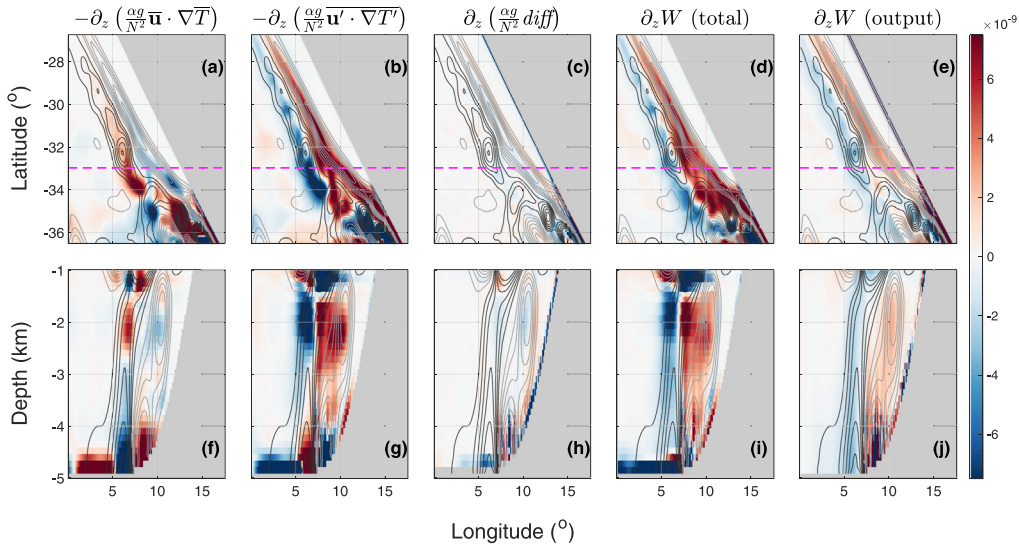


Fig. 6. Analyzing the source of the vortex stretching term, showing vertical derivative of w reconstructed from different terms in the temperature budget. Upper panels: horizontal maps at 2.2 km depth. Lower panels: zonal sections at 33°S. (a,f) temperature advection by the mean flows; (b,g) temperature advection by eddies; (c,h) explicit temperature diffusion (parameterized eddy mixing); (d,i) Sum of mean-flow advection, eddy advection and explicit diffusion; (e,j) vertical derivative of the vertical velocity from the model output. The dark gray contours are northward v -velocity, and the light gray contours are southward v -velocity. The contours are drawn for v -velocity of magnitudes between 0.25 cm/s and 1.5 cm/s, with an interval of 0.25 cm/s. The purple lines in the upper panels show the latitudes of the zonal sections.

transport which shows a local maximum in the core of the current (shading in panels b and g). This again is consistent with the findings of YTS, and because the only eddy effects included here are due to the rings, we can conclude that the vortex stretching driving the DEBC is forced by these rings. In the “Flat bottom+rings” case, without the

slope, the propagation of the Agulhas-like rings is more zonal compared to the “Slope+rings” case, and therefore the contribution of eddy fluxes is concentrated southward of 34°S rather than along the entire eastern boundary. As a result, the flow is also concentrated only near the

southern boundary, demonstrating the importance of the slope to the direction of propagation of the rings and thus to the DEBC.

As a side comment, we note that the combined analysis of the vorticity and temperature budgets used here, is used also in the derivation of quasi-geostrophic potential vorticity (QGPV, $Q = \zeta + \beta y + f \partial_z(\rho' / \partial_z \bar{\rho})$) equation. The dominance of the vortex stretching term in our vorticity budget, and that of the eddy advection in the temperature budget, are together equivalent to a dominance of eddy advection of the QG stretching term $f \partial_z(\rho' / \partial_z \bar{\rho})$ in the QGPV budget. This eddy QGPV advection would take the form $-\nabla \cdot \bar{\mathbf{v}}' S'$, where $S = f \partial_z(\rho' / \partial_z \bar{\rho})$. We can now use $\rho' / \partial_z \bar{\rho} = \eta'$, where η' is the isopycnal height anomaly, and $\partial_z \eta' \approx h' / \bar{h}$, where h' is the deviation of an isopycnal layer thickness from its long term mean \bar{h} . The QG stretching term is therefore approximately equal to $f \nabla_H \cdot \bar{\mathbf{v}}' h' / \bar{h}$, and the entire term is referred to as “eddy thickness advection” (Seville et al., 2012). Supplementary Fig. 8 shows that indeed both the eddy vorticity transport and the eddy thickness advection are important in balancing the βv term in the QGPV budget (panels b,f,d,h), consistent with Seville et al. (2012).

To summarize our goals and findings from the vorticity budget. First, by selectively adding idealized Agulhas rings to the southern boundary condition, as well as a slope topography, we are able to show here that both are important for the vortex stretching signal driving the time-mean DEBC. Second, previous idealized configurations of the Atlantic DEBC found an unrealistic bottom-intensified flow structure (Yang et al., 2020b, 2021). We find here that the reason for the wrong vertical structure is the lack of the Agulhas rings propagating from the southern boundary. We find that the Agulhas rings lead to a stretching signal with a mid-depth maximum which give our “Slope+rings” case its realistic mid-depth centered structure, similar to the observed one. Finally, we are able to decipher the role played by the slope topography: it sets the direction of propagation of the rings, allowing them to induce the near boundary effects that drive the DEBC. This new insight helps explain the results of the realistic simulations of the southeast Atlantic DEBC by Yang et al. (2020a). This is also different from the scenario in the idealized simulations in Yang et al. (2021) where the topography itself is the source of stretching by interaction with bottom flows.

4. Conclusions

Deep Eastern Boundary Currents are observed in multiple Southern Hemisphere ocean basins, and they are important branches of the global meridional overturning circulation (Robbins and Toole, 1997; Sloyan and Rintoul, 2001; Wijffels et al., 2001; Arhan et al., 2003). In particular, the southward NADW transport in the southeast Atlantic Ocean carries significant fluxes of mass, tracers and potential vorticity toward the Southern Ocean (Saunders and King, 1995; Speer et al., 1996; Arhan et al., 2003; Yang et al., 2020a). This DEBC is fed by a broad southeastward interior flow toward the eastern boundary that was found to be driven by eddy thickness fluxes due to the energetic Agulhas rings (Seville et al., 2012). Our focus in this work was the continuation of this flow, the DEBC that is found closer to the eastern boundary of the South Atlantic Ocean. Previous work (Yang et al., 2021, 2020a,b) used both realistic and idealized model configurations, prescribed the inflow and outflow of the Southern Hemisphere DEBCs and examined the dynamical balances of these currents away from the inflow and outflow. Our objectives here were to understand (1) what controls the vertical structure of the South Atlantic DEBC that was not possible to simulate correctly in the previously used idealized configurations which did not include the Agulhas Rings; (2) what is the role of topography in the presence of the rings.

We used an idealized-configuration general circulation model of the South-Atlantic DEBC driven by Agulhas ring-like signal on the southern boundary. We find that only when a sloping bathymetry and the Agulhas-like ring signals are included, does a concentrated southward flow develop along the entire eastern boundary between one and four

kilometers depth, similar to that in the Southern Ocean State Estimate solution. When we use a flat bottom bathymetry, a strong DEBC is observed only in a small latitudinal range, southward of 34°S. When no idealized Agulhas rings are forced, no DEBC can develop. Other experiment with added surface forcing showed that it is indeed the idealized Agulhas rings, rather than eddies forced at surface, that drive the DEBC.

We find that the mid-depth South Atlantic DEBC is mainly forced by vortex stretching that is driven by eddy temperature transport. The vortex stretching driving of the DEBC is found to be due to eddy thickness fluxes which are dominated by the Agulhas rings whose path is set by the topography. This complements the conclusion of Seville et al. (2012) who found that eddy thickness fluxes drive the broad flow which feeds the DEBC studied here. We also find another bottom-intensified branch of the southward flows, similar to one that exists in the SOSE solution and discuss its dynamics in the supplementary material.

There are several caveats to note. First, the broad inflow from the western boundary and the no flow condition imposed on the northern boundary are overly simplified, although motivated by the general structure of the SOSE solution. Second, the representation of the Agulhas-like rings is highly idealized, and in particular ignores higher frequency and smaller spatial scales, and any irregularities. This idealization is intended, because we wanted to find out if a realistic DEBC still develops without the boundary forcing of small scales. The fact that a DEBC still develops (Fig. 1a,e) suggests that the essential boundary forcing is captured by the idealized rings and that smaller boundary scales may not be critical to the driving of the South Atlantic DEBC. As a final caveat we mention that our resolution of about 10 km is insufficient for resolving submesoscale variability that is known to dominate near-surface eastern boundary regions (Peliz et al., 2003; Capet et al., 2008; Cessi and Wolfe, 2009; Colas et al., 2011; Kurian et al., 2011; Bire and Wolfe, 2018), although this variability may not be expected to play a role at a depth of 2.5 km which is the focus here. In summary, it seems that the regional and idealized model configurations used here make a strong case for the driving of the southeast Atlantic DEBC by the Agulhas rings with an important role played by the slope topography to determine the path of such rings.

CRedit authorship contribution statement

Xiaoting Yang: Designed cases 1–4 in this manuscript and did the budget analysis that revealed the most important message conveyed by this paper. The cases added after the first round of review were designed, Numerical experiments and calculations, Writing and revision of this manuscript. **Eli Tziperman:** The cases added after the first round of review were designed, Funding and computational resources, Writing and revision of this manuscript.

Declaration of competing interest

The authors declare that they have no known competing financial interests or personal relationships that could have appeared to influence the work reported in this paper.

Acknowledgments

This work was supported by the National Science Foundation, USA physical oceanography program, grant OCE-1535800. We would like to acknowledge high-performance computing support from Cheyenne provided by NCAR, USA’s Computational and Information Systems Laboratory, sponsored by the National Science Foundation, USA. ET thanks the Weizmann Institute for its hospitality during parts of this work.

The MITgcm 3d ocean model used for this work is a community-developed model available for download from <http://mitgcm.org/>

[public/source_code.html](#). All data, MITgcm modifications, vorticity model codes, and analysis scripts used in this work, are archived in the “Open Science Framework”, which is a public, community-supported repository, at <https://osf.io/agtmq/>. These codes are publicly available, with no restrictions. Southern Ocean State Estimate Data set used in this paper can be found at <http://sose.ucsd.edu>.

Appendix A. Supplementary data

Supplementary material related to this article can be found online at <https://doi.org/10.1016/j.ocemod.2021.101817>.

References

- Arhan, M., Mercier, H., Park, Y.-H., 2003. On the deep water circulation of the eastern south atlantic ocean. *Deep Sea Res. Part I* 50 (7), 889–916.
- Bire, S., Wolfe, C.L., 2018. The role of eddies in buoyancy-driven eastern boundary currents. *J. Phys. Oceanogr.* 48 (12), 2829–2850.
- Böning, C.W., Schott, F.A., 1993. Deep currents and the eastward salinity tongue in the equatorial atlantic: Results from an eddy-resolving, primitive equation model. *J. Geophys. Res. Oceans* 98 (C4), 6991–6999.
- Capet, X., McWilliams, J.C., Molemaker, M.J., Shchepetkin, c.F., 2008. Mesoscale to submesoscale transition in the california current system. part I: Flow structure, eddy flux, and observational tests. *J. Phys. Oceanogr.* 38 (1), 29–43. <http://dx.doi.org/10.1175/2007JPO3671.1>.
- Cessi, P., Wolfe, C.L., 2009. Eddy-driven buoyancy gradients on eastern boundaries and their role in the thermocline. *J. Phys. Oceanogr.* 39 (7), 1595–1614.
- Colas, F., McWilliams, J.C., Capet, X., Kurian, J., 2011. Heat balance and eddies in the peru-Chile current system. *Clim. Dyn.* 39 (1–2), 509–529. <http://dx.doi.org/10.1007/s00382-011-1170-6>.
- Csanady, G., 1978. The arrested topographic wave. *J. Phys. Oceanogr.* 8 (1), 47–62.
- Csanady, G., 1985. “Pycnocathic” currents over the upper continental slope. *J. Phys. Oceanogr.* 15 (3), 306–315.
- Furue, R., McCreary, J.P., Benthuyens, J., Phillips, H.E., Bindoff, N.L., 2013. Dynamics of the Leeuwin Current: Part 1. Coastal flows in an inviscid, variable-density, layer model. *Dyn. Atmos. Oceans* 63, 24–59.
- Gent, P.R., McWilliams, J.C., 1990. Isopycnal mixing in ocean circulation models. *J. Phys. Oceanogr.* 20 (1), 150–155.
- Hogg, N.G., Thurnherr, A.M., 2005. A zonal pathway for NADW in the South Atlantic. *J. Oceanogr.* 61 (3), 493–507.
- Kurian, J., Colas, F., Capet, X., McWilliams, J.C., Chelton, D.B., 2011. Eddy properties in the california current system. *J. Geophys. Res. Oceans* 116 (C8).
- Lumpkin, R., Speer, K., 2007. Global ocean meridional overturning. *J. Phys. Oceanogr.* 37 (10), 2550–2562.
- Marshall, J., Adcroft, A., Hill, C., Perelman, L., Heisey, C., 1997. A finite-volume, incompressible Navier Stokes model for studies of the ocean on parallel computers. *J. Geophys. Res.* 102, 5,753–5,766.
- Mazloff, M.R., Heimbach, P., Wunsch, C., 2010. An eddy-permitting southern ocean state estimate. *J. Phys. Oceanogr.* 40 (5), 880–899.
- Peliz, Á., Dubert, J., Haidvogel, D.B., Le Cann, B., 2003. Generation and unstable evolution of a density-driven eastern poleward current: The iberian poleward current. *J. Geophys. Res. Oceans* 108 (C8).
- Robbins, P.E., Toole, J.M., 1997. The dissolved silica budget as a constraint on the meridional overturning circulation of the Indian ocean. *Deep Sea Res. Part I* 44 (5), 879–906.
- Saunders, P.M., King, B.A., 1995. Oceanic fluxes on the WOCE A11 section. *J. Phys. Oceanogr.* 25 (9), 1942–1958.
- Seville, E., Johns, W.E., Beal, L.M., 2012. Does the vorticity flux from agulhas rings control the zonal pathway of NADW across the south atlantic?. *J. Geophys. Res. Oceans* 117 (C5).
- Sloyan, B.M., Rintoul, S.R., 2001. The Southern Ocean limb of the global deep overturning circulation. *J. Phys. Oceanogr.* 31 (1), 143–173.
- Speer, K.G., Holfort, J., Reynaud, T., Siedler, G., 1996. South atlantic heat transport at 11 S. In: *The South Atlantic*. Springer, pp. 105–120.
- Speer, K.G., Siedler, G., Talley, L., 1995. The namib col current. *Deep Sea Res. Part I* 42 (11–12), 1933–1950.
- Stommel, H., Arons, A., 1959. On the abyssal circulation of the world ocean—II. An idealized model of the circulation pattern and amplitude in oceanic basins. *Deep Sea Res.* (1953) 6, 217IN15219–218IN18233.
- Stramma, L., England, M., 1999. On the water masses and mean circulation of the south atlantic ocean. *J. Geophys. Res. Oceans* 104 (C9), 20863–20883.
- Warren, B.A., Speer, K.G., 1991. Deep circulation in the eastern South Atlantic Ocean. *Deep Sea Res.* 38 (Suppl.), 281–322.
- Weiss, R.F., Bullister, J.L., Gammon, R.H., Warner, M.J., 1985. Atmospheric chlorofluoromethanes in the deep equatorial atlantic. *Nature* 314 (6012), 608–610.
- Wijffels, S.E., Toole, J.M., Davis, R., 2001. Revisiting the South Pacific subtropical circulation: A synthesis of world ocean circulation experiment observations along 32s. *J. Geophys. Res.* 106 (C9), 19481–19513.
- Woodruff, S.D., Slutz, R.J., Jenne, R.L., Steurer, P.M., 1987. A comprehensive ocean-atmosphere data set. *Bull. Am. Meteor. Soc.* 68, 521–527.
- Yang, X., Tziperman, E., Speer, K., 2020a. Deep eastern boundary currents: Realistic simulations and vorticity budgets. *J. Phys. Oceanogr.* 50 (11), 3077–3094.
- Yang, X., Tziperman, E., Speer, K., 2020b. Dynamics of deep ocean eastern boundary currents. *Geophys. Res. Lett.* 47 (1), e2019GL085396.
- Yang, X., Tziperman, E., Speer, K., 2021. Deep eastern boundary currents: idealized models and dynamics. *J. Phys. Oceanogr.*